THE EFFECT OF PARTICLE SORTING ON ^{230}TH SEDIMENT INVENTORIES IN THE EASTERN EQUATORIAL PACIFIC OCEAN

A Thesis

by

RAMI IBRAHIM

Submitted to the Office of Graduate and Professional Studies of
Texas A&M University
in partial fulfillment of the requirements for the degree of

MASTER OF SCIENCE

Chair of Committee,	Franco Marcantonio
Co-chair of Committee,	Mitchell Lyle
Committee Member,	Michael Pope
Head of Department,	Michael Pope

December 2015

Major Subject: Geology

ABSTRACT

The ^{230}Th Method of determining mass accumulation rates (MARs) assumes little to no fractionation during lateral syndepositional processes occurring at the seafloor. We examine ^{230}Th inventories in paired jumbo piston core sediments from paired winnowed and focused sites to radiocarbon-dated multicore sediments at the Carnegie Ridge in the Panama Basin. Radiocarbon-derived coarse content MARs, likely representative of vertical rain of particles poorly transported by sea bottom currents, are spatially and temporally similar, whereas measured xs^{230}Th-derived MARs are lower than age-model-derived MARs at both sites. ^{230}Th-normalization suggests focusing factors ranging from 2 at "thin" site 11JC, and 5 at "thick" site 17JC, with little temporal differences between MIS 1 and MIS 2. ^{230}Th-normalized coarse content shows no temporal or spatial patterns, whereas age-model-derived coarse content yields the expected temporal similarities between both sites. The latter method also suggests higher productivity (higher deposition rates) during MIS 2 compared to those measured during MIS 1. ^{230}Th-normalized measurements of one component of the fine-grained fraction, dust fraction as estimated with the ^{232}Th concentrations, provides evidence for the utility of ^{230}Th constant-flux proxy in highly focused regions in the ocean.

DEDICATION

This thesis is dedicated to my family, my parents, Hani Ibrahim and Dina Metwally, for being a supportive strength in my academic graduate calling. My brother, Seif, who always pushed me to achieve more, and to always strive to better my career and myself.

ACKNOWLEDGEMENTS

First and foremost, I would like to extend gratitude and thanks my research advisor and mentor, Dr. Franco Marcantonio, who has supported and believed in me through the easy times and the hard times. His work ethic is second to none. His passion for teaching is tremendous. He doesn't want you to just learn the material, he wants you to understand it, and given enough time, how you can contribute to it. Through multiple iterations and discussions, Dr. Marcantonio has provided me the analytical and quantitative skills to tackle this highly polarizing issue in radiogenic isotope geochemistry. Through the work compiled and analyzed in this thesis, Dr. Marcantonio and I show that through methodical treatment of sediment water interface core samples, we are able to determine Th isotope processes and sediment accumulation rates in the Eastern Equatorial Pacific Ocean.

Furthermore, I gratefully acknowledge my committee members Dr. Mitch Lyle and Dr. Michael Pope, and the rest of the department for making Texas A&M University a second home. I'd like to thank the lab coordinator Luz Romero for her expertise, guidance, and ability at keeping everything functional. Also I wish to thank Dr. Matthew Schmidt, Jennifer Hertzberg, Kelly Brooks, Julia Shackford, and Cameron Nikmard for their contributions.

NOMENCLATURE

CFP	Constant Flux Proxy
EEP	Eastern Equatorial Pacific
JC	Jumbo Piston Core
kyr	Unit of time equal to 1 thousand years, 10^3 years
MAR	Mass Accumulation Rate
MC	Multicore
MIS	Marine Isotope Stage
MV	Melville Cruise
ybp	Years before present

TABLE OF CONTENTS

LIST OF FIGURES

Page

LIST OF TABLES

Page

1. INTRODUCTION

Sedimentary mass accumulation rates (MARs) in the deep ocean are crucial to studies of paleoceanography and paleoclimatology. MARs, which are burial fluxes of sedimentary material at the seafloor, typically change in direct response to changes in climate. For example: 1) increases in biological production, $CaCO_3$, coming from an increase in planktic foraminifer, in the surface ocean (and consequent increases in rates of carbon burial) may result in a decrease of atmospheric CO_2, which can result in cooling of the planet; or 2) increases in the flux of wind-blown detrital material deposited the deep ocean may be related to changes in atmospheric circulation which, in turn, can regulate the transport of heat from the equator to the poles.

The standard MAR calculation by multiplying the linear sedimentation rate between dated horizons (LSR, increase in sediment thickness per unit time) with the sediment dry bulk density. The time horizons can be dated directly using radiocarbon analysis, or are indirectly estimated using oxygen-isotope stratigraphy or other stratigraphic correlation techniques to date horizons. This method of calculating sediment mass accumulation rates does not differentiate between sediments that were derived vertically (i.e., rained through the water column) from those that were redistributed horizontally by lateral deep ocean currents.

Another technique for calculating MARs is known as the Constant-Flux Proxy (CFP) method (Suman and Bacon, 1989). The CFP method of calculating MARs assumes that

the flux of one sedimentary component to the seafloor is known and constant. By simply measuring the concentration of this component in an interval of sediment the MAR can be calculated (Suman and Bacon, 1989). ^{230}Th commonly is used as a constant-flux proxy essentially because of its distinct geochemical behavior in the ocean. ^{230}Th, which has a short residence time (decades; Bacon and Anderson, 1982) in the ocean because of its insolubility, is produced by the decay of its parent, ^{234}U, which has a long residence time (~400 kyr, Henderson; 2002) and is homogenously distributed throughout the ocean. When an atom of ^{230}Th is produced by the decay of ^{234}U, the thorium will be rapidly scavenged onto water column particles, which then settle to the seafloor. Hence, the sediment deposited on the seafloor will have an excess of ^{230}Th that is not in equilibrium with the ^{234}U in the sediment. It is assumed that the flux of ^{230}Th falling to the ocean floor matches the rate of production of ^{230}Th in the water column directly above it due to the decay of dissolved ^{234}U (Bacon, 1984). Therefore, by dividing the known production rate of ^{230}Th by the ^{230}Th concentration within a specific interval of sediment one can calculate the sediment MAR for that same interval. When it was realized that deposition rates of Th-230 frequently exceeded production rates in the water column, it was suggested that the added Th-230 was a measure of horizontal advection and deposition of sediment (Francois et al, 2004, or variety of references) and could be used to normalize away the horizontally redistributed component.

In the eastern equatorial Pacific (EEP), marine sediment MARs calculated using the two methodologies outlined above are significantly different. Specifically, sediment MARs near the equator calculated using the standard approach are always significantly greater

than those calculated using the ^{230}Th CFP method (e.g., Marcantonio et al., 2014; Singh et al., 2011; Francois et al., 2007; Kienast et al., 2007; Loubere et al., 2004; Lyle et al., 2005, 2007). In addition, the proportional difference between the two techniques is greater for sediment deposited during the last glacial interval (11500-25000 ybp) than those deposited during the Holocene.

This dramatic difference is explained by invoking focusing, i.e., the lateral redistribution of sediment by deep-sea currents. Proponents of the ^{230}Th technique suggest that by dividing the inventory of ^{230}Th within an interval of sediment, for which a known amount of ^{230}Th should be present, a sediment "focusing factor (ψ)" (Suman and Bacon, 1989; Francois et al., 2004) can be calculated. Focusing Factors are calculated using the following formula:

$$\psi = \frac{\int_{r1}^{r2}(^{230}Th_{xs,0})\rho_r dr}{\beta z(t_1 - t_2)} \ldots (1)$$

where r_1 and r_2 are sediment depths (cm), ρ_r is mean dry bulk density (g/cm^3), t_1 and t_2 are the corresponding sediment ages (kyr) for intervals r_1 and r_2, β is the production of ^{230}Th from ^{230}Th decay in the water column (0.0267 $\frac{dpm}{m^3 yr}$) and z is the water depth (m). The $xs^{230}Th_0$ and ρ_r are averaged over the depth interval z_1 to z_2 in the sediment core. When ψ>1, there is additional sediment that is being transported to the site laterally by deep-sea currents, while ψ<1 suggests that sediments are being winnowed from the site. In the EEP, ψ is almost always greater than 1 with the largest factors being ~4-

5(Marcantonio et al., 2014; Singh et al., 2011: Kienast et al., 2008) at the equator and slightly south of the equator close to the Carnegie Ridge in the Panama Basin.

Such high sediment focusing factors suggest that greater than 80% of the sediments in some regions of the Panama Basin were transported there via lateral sediment redistribution along the seafloor rather than by falling vertically by raining through the water column. Some suggest the assumptions inherent in the ^{230}Th methodology are not valid and, that, therefore, interpretations of sediment focusing are exaggerated (Lyle et al., 2005; Lyle et al., 2007). The purpose of this thesis is to study the inventories of ^{230}Th in the Panama Basin close to the Carnegie Ridge. We look in detail at the focusing process by analyzing new cores from near the Carnegie Ridge in the Panama Basin, where ^{230}Th-derived focusing factors are the highest in all of the Pacific Ocean. We compare our ^{230}Th record to those calculated by Singh et al. (2011) in similar regions of the Panama Basin and to those determined by Marcantonio et al. (2014) in some of the same multicores studied here. Our main emphasis will be to investigate particle sorting and how it affects ^{230}Th inventories in the Panama Basin over the past 25 kyr.

2. METHODOLOGY

2.1 Sampling and age models

We sampled piston cores collected during an oceanographic research expedition in November 2010 (R/V Melville cruise MV1014). During this cruise, seismic surveying identified thicker-than-average sediment packages in regional basins that were potentially focused, and thinner-than-average sediment packages closer to ridge tops that were potentially winnowed. We concentrate on material retrieved from the Carnegie Ridge (for location see Table 1, Figure 1), and compare ^{230}Th inventories at (1) an apparently winnowed site on the north flank of Carnegie Ridge but where sediments still accumulate (MV1014-11JC and 9 MC), (2) a site at the base of Carnegie Ridge where excess sediments seem to have accumulated (MV1014-12JC; not compared in this paper), and a site on an abyssal hill near the equator but beyond the basin at the foot of the Carnegie Ridge (MV1014-17JC).

In order to calculate meaningful ^{230}Th inventories good age control is required. Sedimentary mass accumulation rates (MAR) are estimated by multiplying sediment dry bulk density with the linear sedimentation rate (LSR), calculated using dated sediment horizons which are typically derived from δ^{18}O tie-point stratigraphy, volcanic ash chronology, correlation to nearby well-dated cores, or from ^{14}C dating.

$$Bulk\ MAR = \rho_{dry} \times LSR$$

where $LSR = (z_2 - z_1)/(t_2 - t_1)$ (cm/kyr) and ρ_{dry} is the dry bulk density (g/cm^3), z_1 and z_2 are sediment horizon depths 1 and 2 respectively (cm), and t_1 and t_2 are the corresponding sediment ages (kyr). The MAR of a sediment component like $CaCO_3$ is achieved by multiplying the bulk MAR by the weight fraction of the component in the sediment (e.g., 0.85 for a sediment with 85% $CaCO_3$).

To help construct age models, oxygen isotope analyses of specimens of the planktic foraminifer, *N. dutertrei*, were picked from the >250 μm fraction of samples taken every 20 cm starting from the top of the piston cores. The foraminifer samples were analyzed in the laboratory of Dr. Jean-Lynch Stieglitz at the Georgia Institute of Technology. The oxygen isotope analysis allowed marine isotope stage boundaries MIS 1-MIS 2 (11500 ybp) and MIS 2-MIS 3 (25000 ybp) to be determined in piston cores 11JC and 17JC (Table 2, Figures 2 and 3).

Additional age tie-points were obtained by correlating $CaCO_3$ concentrations in our piston core sediments with variations in $CaCO_3$ concentrations in a nearby well-dated core (ME0005-24JC; Kienast et al,. 2007). High-resolution XRF Ca analysis of core material was effectively used as a proxy for calcium carbonate concentrations (Lyle et al., 2012). Our piston cores (11JC, 12JC, 17JC) were scanned by an X-ray fluorescence (XRF) spectrometer at the Integrated Ocean Drilling Program (IODP) Gulf Coast Repository at the Texas A&M University campus. Each core was scanned at 10 mm intervals at 10 kV and scanned again at 50 kV. Both runs scanned for the following elements: Al, Si, P, S, Cl, Ar, K, Ca, Ti, Cr, Mn, Fe, Rh, and Ba. Raw Ca peak areas are

first scaled to a median component concentration and then summed. The sum is normalized to 100%, using the equation

$$NMS_C = C \times 100/(raw\ sum) \ldots (2)$$

where NMS_c is the normalized median-scaled value for the component and C is the median-scaled value of that component (Lyle et al,. 2012). A regionally abundant ash layer deposited at 84 ka (Drexler et al., 1980) was also used to correlate the various core depths to each other. This ash layer occurs at 829.6 cm in core 12JC, 954.7 cm in core 17JC, and 386.8 cm in core 11JC and 980 cm in 24JC. Together, the Ca (proxy for $CaCO_3$) correlations, the ash layer chronology and the oxygen isotope stratigraphy (Figures 2, 3, and 4) are used to generate a general chronological framework for 11JC, 12JC, and 17JC (Table 3).

2.2 Radionuclide isotope measurements

Individual sediment intervals were sampled and dried (1-2 days) in the laboratory oven. After being homogenized with a mortar and pestle, 0.3-0.4 g of each sediment sample was spiked with known amounts of ^{229}Th and ^{236}U. The samples were then digested with a series of acids ($HClO_4$, HNO_3, HF, and HCl). After dissolution, NH_4OH was added to each sample (to generate a pH between 7 and 8) in order to precipitate Fe oxyhydroxides, onto which thorium and uranium are scavenged.

The oxyhydroxide precipitates were centrifuged, washed, and then dissolved in hydrochloric acid, at which point, the samples were processed via traditional ion

exchange chromatography for U and Th. The purified U and Th were analyzed on the Element XR high-resolution inductively-coupled plasma mass spectrometer (HR-ICP-MS) at TAMU. Procedural blanks were analyzed throughout the course of this study and were insignificant, so that blank corrections were unnecessary.

3. RESULTS

3.1 Age-model-derived sedimentation rates

The $\delta^{18}O$ analysis for core 11JC suggests that of the interval of sediment deposited during MIS 1 is from 0 to 48 cm (Figure 2). This corresponds to a linear sedimentation rate of about 4 cm/kyr. The sedimentation rate during the same interval for core 17JC is about 3 times as great (i.e., 12 cm/kyr) since the boundary between MIS 1 and MIS 2 occurs deeper at 148 cm (Figure 3). MIS 2 spans 48 cm to 147 cm for 11JC, and 148 cm to 436 cm for 17JC. This suggests double the sedimentation rate for both cores during MIS 2 compared to that determined for MIS 1 (i.e., 8 and 24 cm/kyr for 11JC and 17JC, respectively). The 3-fold greater sedimentation rate at 17JC compared to that at 11JC is consistent with the seismic identification of a thicker sediment package at the down-slope position of core 17JC (Figure 3).

3.2 ^{230}Th-derived sediment mass accumulation rates

^{230}Th-derived MARs for 11JC were, on average, 1.7 g/cm^2/kyr during MIS 1 and 2.6 g/cm^2/kyr during MIS 2 (Figure 5 and Table 4). The lower ^{230}Th-derived accumulation rates, compared to those derived using the age model, are suggestive of significant focusing, during both time periods even at this up-slope, more slowly deposited site. Core 17JC had ^{230}Th-derived MARs of 1.5 g/cm^2/kyr during MIS 1, and 1.8 g/cm^2/kyr during MIS 2 (Figure 5 and Table 4). Age-model-derived MARs are much higher at this

site compared to those derived using the ^{230}Th technique, and suggest significant amounts of focusing at this seismically-identified “thick” site.

3.3 Sediment coarse fraction

The coarse fraction (>63μm) was measured for piston cores 11JC and 17JC at evenly spaced depth intervals throughout MIS 1 and MIS 2. For core 11JC, during MIS 1, the coarse fraction ranged from 27.5% to 35.5%, with an average of 31.9% (Table 5). For the same core, during MIS 2, coarse fractions were higher and ranged between 58.1% and 77.2%, with an average of 67.6%. Coarse fractions for 17JC ranged from 18.5% to 21.5%, with an average of 20.4%, and from 19.6% to 22.2%, with an average of 20.9%, during MIS 1 and MIS 2, respectively (Table 5). Holocene coarse fraction values for both piston cores are in agreeance well with paired multicore data (Marcantonio et al., 2014).

4. DISCUSSION

4.1 Differences between MAR estimates, focusing factors, and estimates of export production

A comparison of the accumulation rates derived using the two methodologies (^{230}Th-derived versus age-model-derived) at both the thick (down slope) and thin sites (up slope) reveals significant inconsistencies (Figures 5 and 6). While the ^{230}Th-derived accumulation rates show minimal variability both spatially and temporally (Figure 5), the age-model-derived accumulation rates are more variable (Figure 6) at both scales. The differences in the two methodologies lead to a determination of the ^{230}Th-derived focusing factors (see equation 2 above). In a study of Carnegie multicores, which are paired with the piston cores studied here (9MC with 11JC, and 16MC with 17JC), it was suggested, using ^{230}Th-derived focusing factors, that focusing of sediments occurred both close to the ridge top (9MC) and downslope from the ridge (16MC) (Marcantonio et al., 2014). The up-slope, low sedimentation rate site (11JC) has ^{230}Th-derived sediment focusing factors of about 2 (similar to the value of 1.5 at 9MC) during both MIS1 and MIS 2 (Figure 7, Table 6). Focusing factors at the down-slope, high sedimentation rate site (17JC) are significantly higher during both MIS 1 (4.8) and MIS 2 (5.8) (Figure 7, Table 6) being two of the highest recorded in the equatorial Pacific. This analysis of lower (9MC, 11JC) versus higher (16MC, 17JC) ^{230}Th-derived sediment focusing factors is consistent with the sediment isopach map since the ash layer deposited at 84 ka (Figure 18, Brooks, 2014) and with the relative position of the ash layer in the analyzed cores (Figure 4).

The ^{230}Th technique of estimating sediment mass accumulation rates (MARs) was assessed recently and determined that for regions in which sediment focusing by deep-sea currents is known to occur there can be significant fractionation of fine particles from coarser particles (Marcantonio et al., 2014). Such fractionation can bias ^{230}Th-derived MARs such that they are inaccurate representations of vertical deposition rates. Marcantonio et al. (2014) suggested that age-model-derived MARs of the coarse-grained fraction may be a better representation of the rate of particles falling from the surface ocean in regions of the seafloor in which sediment was redistributed laterally by deep-sea currents. Since the >63 μm fraction of the sediment is unlikely to be as affected by such currents (i.e. 20-25 m/s needed, McCave et al., 2006), the age-model-derived MARs of this fraction should reflect the true vertical deposition rates. In the absence of grain size fractionation, as is assumed in the ^{230}Th technique, one would expect little difference in the relative variability of ^{230}Th-derived MARs and age-model-derived vertical deposition rates.

The age-model-derived coarse content accumulation rates are plotted in Figure 8. The two most important features are that the coarse content accumulation rates are a) similar at both the thin (11JC) and thick (17JC) sites during the same time intervals (i.e., MIS 1 and MIS 2), and b) are 2.5-3 times higher during MIS 2 than those determined during MIS 2. The similar deposition rates measured at each site during the same time period are to be expected given the proximity (~54 km) of sites 11JC and 17JC (Figure 1). More importantly, however, is that the higher vertical deposition rates are likely indicative of greater primary production during MIS 2 in this region of the EEP. While

some EEP studies based on MARs suggest there were greater fluxes during glacial events (Lyle et al., 2002; Paytan et al., 2004), others shows minor glacial to interglacial variations in the fluxes (Marcantonio et al., 2001; Higgins et al., 2002; Loubere et al., 2004).

Notably, the ^{230}Th-derived MARs (Figure 5), which are thought to reflect vertical deposition rates, have some semblance to the patterns observed in age-model-derived coarse content accumulation rates (Figure 8). For example, at both sites 17JC and 11JC during MIS 1, similar ^{230}Th-derived MARs are observed despite the greater than factor of 2 difference in sediment focusing factor. Although at 11JC, the average ^{230}Th-derived MAR during MIS 2 is higher than that derived during MIS 1, the extent of the increase of the apparent rain rate (~60%) is significantly lower than the 3-fold difference indicated by age-model-derived coarse content accumulation rate. At 17JC, there is little difference between the ^{230}Th-derived MARs measured during MIS 1 and MIS 2 in contrast to the 2.5-fold difference measured in the age-model-derived coarse content accumulation rates. Furthermore, the MIS 2 average ^{230}Th-derived MAR for 17JC is significantly lower than the rate measured during the same time period for 11JC. Given the proximity of the two sites, this is an unexpected result if ^{230}Th-derived MARs are representing true vertical deposition rates. Apparently, the likelihood of size fractionation effects that result in ^{230}Th-derived MARs that are not representative of true MARS is greatest in regions that have undergone the greatest degree of sediment redistribution.

4.2 Constraints on ^{230}Th fluxes due to grain size fractionation effects

Dissolved thorium in the water column is highly particle reactive and gets preferentially scavenged onto fine-grained silt and clay-sized particles (Kretschmer et al., 2010). This is due to the greater number of reactive surfaces on the smaller particles. For example, it was suggested that more than 90% of the total thorium is in grains <20 μm in size (Kretschmer et al., 2010). On the other hand, only 2-4 % of all $^{230}Th_{xs}$ was in the coarse-grained fraction (i.e., >63 μm). Once the fine particles settle to the seafloor they can be resuspended and transported depending on the velocity of the bottom currents. It is highly unlikely that the coarse fraction would be redistributed by the typical weak currents in the deep sea (Masson et al., 2004, McCave et al., 2006). Oddly, in a study of drift deposits of the Blake Nose in the North Atlantic, that although the sediments contained enhanced concentrations of fine-grained particles (i.e., likely redistribution has occurred) the ^{230}Th systematics were not disturbed (McGee et al. 2010). They explained this by pointing to the potential cohesive effect that moderate-strong currents have on the <10 μm grain size fraction (McCave, 2008). This hypothesis led Marcantonio et al. (2014) to a suggestion that weak bottom currents, such as those influence by tidal action in the Panama Basin (1-2 cm/s, Gardner et al., 1984), are actually better at separating the fine- from the coarse-grained sediments (Marcantonio et al., 2014). Similarly, data from the central equatorial Pacific suggests a ^{230}Th-enriched nepheloid layer near the sea floor that causes enhanced apparent deposition in sediment traps within 500 m of the bottom (Lyle et al., 2014).

Lateral focusing of sediments at the Carnegie Ridge sites likely fractionates the fine-grained and coarse-grained sediments and, in the process causes artifacts in the ^{230}Th-derived MARs. Given the greater concentration of ^{230}Th in fine particles, sediments that have undergone significant focusing and, thus, fractionation of the fines, should produce ^{230}Th-derived MARs that are lower than the actual MARs. At 11JC, where the sediment pile is not as thick, ^{230}Th inventories are higher than those expected from water column production alone, but only by two-fold. In contrast, at 17JC (thick site), ^{230}Th inventories are about five times than those estimated from water production. One would expect, therefore, a greater underestimation of true MARs at the 17JC site, than that at the 11JC site. A comparison between the ^{230}Th-derived MARs and the age-model-derived coarse content MAR should help address the likelihood of this expectation. Indeed, the pattern of changing MARs between MIS 1 and MIS 2 at 11JC is similar for both ^{230}Th- and age-model-derived coarse content MARs (Figures 8 and 9). That is, an approximate two-fold increase from Holocene to glacial is determined for both deposition rate estimations. On the other hand, at 17JC, the ^{230}Th-derived MARs are lower than those derived for 11JC during MIS 1 and MIS 2. Furthermore, the pattern of a significant increase in deposition rates from MIS 1 to MIS 2 is not observed in the ^{230}Th-derived MARs, as they are in the age-model-derived coarse content MARs (Figures 5 and 6). It is likely, therefore, that the ^{230}Th-derived MARs are significantly underestimated at 17JC, the thicker site with the greatest focusing.

^{230}Th-derived MARs underestimate ^{230}Th-derived fluxes of the coarse content (Figure 9) by 50%, at the slightly focused site of 11JC, to an order of magnitude, at the highly

focused site of 17JC. These results are similar to those determined for the multicores 9MC and 16MC (Marcantonio et al., 2014). Previous work, which normalized $CaCO_3$ content (predominantly in the coarse-grained fractions) to ^{230}Th concentrations may need to be rethought if the study areas had undergone significant sediment focusing (Marcantonio et al., 2014). On the other hand, those fine-grained components of the sediment (including the dust, barite, and opal contents) have ^{230}Th-derived fluxes that are likely meaningful, at least in a qualitative manner (Marcantonio et al., 2014). Here we corroborate this conclusion in our determination of the ^{230}Th-derived ^{232}Th (a proxy for the sedimentary lithogenic dust component) fluxes. In Figure 10 we plot these fluxes for both MIS 1 and MIS 2 at both Carnegie sites. If the ^{230}Th-derived ^{232}Th fluxes were to represent the rain of dust falling through the water column at each site, one would expect the temporal slices of these values to be similar. This expectation is based on the proximity of the sites (~54 km apart) and the nature of the relative homogeneity of dust fallout over the ocean. For the Holocene, the difference between ^{232}Th fluxes at 11JC and 17JC is only about 16%. Similarly, during MIS 2, the difference between the same fluxes at the sites is also approximately 20%. Assuming the ^{232}Th fluxes represent dust fluxes, it is important to note that the temporal variability in dust flux from the last glacial to the Holocene is small, being 35% smaller at the position of 17JC, and 2% temporal variability at 11 JC.

5. CONCLUSIONS

In the Panama Basin, measured xs^{230}Th-derived MARs (excess) are lower than age-model derived MARs at two sites, one that has a thin and the other a thick sediment pile. Normalization to ^{230}Th concentrations suggests focusing factors that range from about 2 (thin site, 11JC) to 5 (thick site, 17JC), with little difference in these factors on glacial-interglacial timescales. The coarse content at each of these sites should be representative of the preserved deposition of particles from the surface since these particles are large enough that typical tidal deep-sea currents (1-2 cm/s, Gardner et al., 1984) in the Panama Basin are likely unable to transport them. However, when these coarse contents are normalized to ^{230}Th concentrations, the results are erratic with no spatial or temporal patterns observed. On the other hand, normalizing the coarse content to the age-model-derived MAR produces the expected result of similar rain rates at both sites despite the greater extent of focusing at the thick (17JC) compared to the thin (11JC) site. Additionally, using the latter method suggests greater deposition rates (higher productivity) during the last glacial compared to those measured during the Holocene. Compared to the results for the coarse-grained fraction of the sediment, ^{230}Th-normalized measurements of one component of the fine-grained fraction (the dust fraction as estimated with the ^{232}Th concentrations) provide evidence for the usefulness of ^{230}Th constant-flux proxy in highly focused regions in the ocean.

REFERENCES

1. Bacon, M. P., Anderson, R. F. (1982) Distribution of Thorium isotopes between dissolved and particulate forms in the deep-sea, *Journal of Geophysical Research,* 87, pp. 2045-2056.
2. Bacon, M. P. (1984), Glacial to interglacial changes in carbonate and clay sedimentation in the Atlantic Ocean estimated from 230 Th measurements, *Isot. Geosci*., 2, pp. 97–111.
3. Broecker, W. (2008), Excess sediment 230Th: Transport along the sea floor or enhanced water column scavenging?. *Global Biogeochem., Cycles, 22,* GB1006, doi:10.1029/2007GB003057.
4. Drexler, J. W., W. I. Rose Jr., R. S. J. Sparks, and M. T. Ledbetter (1980) The Los Chocoyos Ash, Guatemala: A major stratigraphic marker in middle America and in three ocean basins, *Quat. Res*., 13, pp. 327–345.
5. Francois, R., Frank, M., Rutgers van der Loeff, M.M., Bacon, M.P., (2004) 230Th normalization: an essential tool for interpreting sedimentary fluxes during the late Quaternary. *Paleoceanography,* 19, PA1018.
6. Francois, R., et al., (2007) Comment on "Do geochemical estimates of sediment focusing pass the sediment test in the equatorial Pacific?" by M. Lyle et al. (2005). *Paleoceanography,* 22, PA1216.
7. Henderson, G. M. (2002) Seawater (234U/238U) during the last 800 thousand years, *Earth and Planetary Science Letters,* 199, pp. 97-110.

8. Higgins, S. M., Broecker, W., Anderson, R., (1999), Enhanced Sedimentation along the Equator in the Western Pacific. *Geophysical Research Letters*, 26, 3489-3492.
9. Higgins. S. M., Anderson, R. F., Marcantonio, F., Schlosser, P., Stute, M. (2002) Sediment focusing creates 100-ka cycles in interplanetary dust accumulation on the Ontong Java Plateau. *Earth and Planetary Science Letters*, 203, pp. 383-397.
10. Kienast, S.S., Kienast, M., Mix, A.C., Calvert, S.E., Francois, R., (2007) Thorium-230 normalized particle flux and sediment focusing in the Panama Basin region during last 30,000. *Paleoceanography*.
11. Kretschmer S., Geibert, W., Rutgers van der Loeff, M. M., Mollenhauer, G., (2010), Grain size effects on 230Thxs inventories in opal-rich and carbonate-rich marine sediments. *Earth and Planetary Science Letters*, 294, pp. 131-142.
12. Kretschmer S., et al., (2011), Fractionation of 230Th, 231Pa, and 10Be induced by particle size and composition within an opal-rich sediment of the Atlantic Southern Ocean. *Geochimica et Cosmochimica Acta*, 75, pp. 6971-6987
13. Loubere, P., Mekik, F., Francois, R., Pichat, S., (2004). Export fluxes of calcite in the eastern equatorial Pacific from the Last Glacial Maximum to the present. *Paleoceanography*, 19, PA2018.
14. Lyle, M., Mix, A., Pisias, N. (2002). Patterns of $CaCO_3$ deposition in the eastern tropical Pacific Ocean for the last 150 kyr: Evidence for a southeast Pacific depositional spike during marine isotope stage (MIS) 2. *Paleoceanography*, 17, doi: 10.1029/2000PA000538.

15. Lyle, M., Mitchell, N., Pisias, N., Mix, A., Martinez, J.I., Paytan, A., (2005). Do geochemical estimates of sediment focusing pass the sediment test in the equatorial Pacific? *Paleoceanography*, 20, PA1005.
16. Lyle, M., Pisias, N., Paytan, A., Martinez, J.I., Mix, A., (2007). Reply to comment by R. Francois et al. on "Do geochemical estimates of sediment focusing pass the sediment test in the equatorial Pacific?": further explorations of ^{230}Th normalization. *Paleoceanography*, 22, PA1217.
17. Lyle, M., A., Lyle, N., T., Gorgas, A., Holbourn, T., Westerhold, E., Hathorne, K., Kimoto, S., Yamamoto, (2012) Data report: raw and normalized elemental data along the Site U1338 splice from X-ray fluorescence scanning, *Proceedings of the Integrated Ocean Drilling Program*, 320/321, pp. 1-19.
18. Lyle, M., F. Marcantonio, W. S. Moore, R. W. Murray, C.-A. Huh, B. P. Finney, D. W. Murray, and A. C. Mix (2014), Sediment size fractionation and focusing in the equatorial Pacific: Effect on ^{230}Th normalization and paleoflux measurements, *Paleoceanography*, 29, 747–763, doi:10.1002/2014PA002616.
19. Marcantonio, F., Anderson, R. F., Higgins, S., Fleisher, M. Q., Stute, M. Schlosser, P. (2001). Abrupt intensification of the SW Indian Ocean monsoon during the last deglaciation: Constraints from Th, Pa, and He isotopes. *Earth and Planetary Science Letters*, 184, pp. 505–514.
20. Masson, D. G., Wynn, R.B., Bett, B. J. (2004) Sedimentary environment of the Faroe-Shetland and Faroe Bank Channels, north-east Atlantic, and the use of

bedforms as indicators of bottom current velocity in the deep ocean, *Sedimentology*, 51, pp. 1207-1241

21. McCave, I. N., and I. R. Hall (2006), Size sorting in marine muds: Processes, pitfalls, and prospects for paleoflow-speed proxies, Geochem. Geophys. Geosyst., 7, Q10N05, doi:10.1029/2006GC001284
22. McCave, I.N., (2008), Size sorting during transport and deposition of fine sediments: sortable silt and flow speed, Developments in Sedimentology, 60, 121-142, doi:10.1016/S0070-4571(08)00208-2
23. Mollenhauer, G., McManus, J. F., Wagner, T., McCave, I. N., Eglinton, T. I., (2011) Radiocarbon and 230Th data reveal rapid redistribution and temporal changes in sediment focussing at a North Atlantic drift. *Earth and Planetary Science Letters*, 301, pp. 373-381.
24. Paytan, A., Lyle, M., Mix, A., Chase, Z. (2004). Climatically driven changes in oceanic processes throughout the equatorial Pacific. *Paleoceanography*, 19, PA4017.
25. Singh, A., Marcantonio, F., Lyle, M., (2011). Sediment focusing in the Panama Basin, Eastern Equatorial Pacific Ocean. *Earth and Planetary Science Letters*, 309, pp. 33–44.
26. Suman, D.O., Bacon, M.P., (1989). Variations in Holocene sedimentation in the North-American basin determined from Th-230 measurements. Deep-Sea Research Part a-*Oceanographic Research Papers*, 36 (6), pp. 869–878.

27. Thompson, J., Colley, S., Anderson, R., Cook, G. T., Mackenzie, A. B., Harkness, D. D., (1993) Holocene sediment fluxes in the northeast Atlantic from 230THexcess and radiocarbon measurements, *Paleoceanography*, 8, pp. 631-650.

APPENDIX A FIGURES

This appendix includes figures to be used in conjunction with the text.

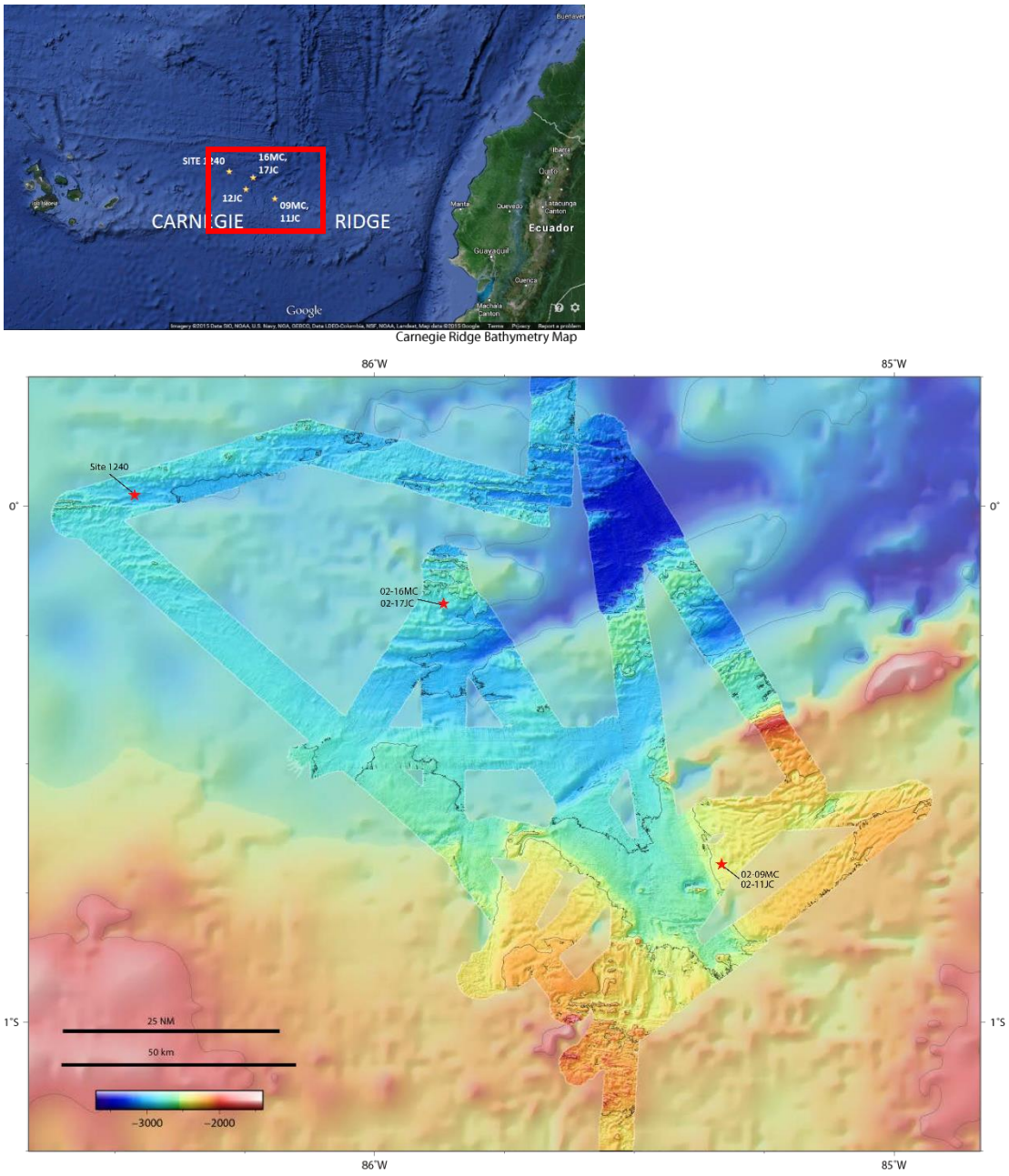

Figure 1. Bathymetry map of the sites in the study area.
24JC is at the same location as IODP Site 1240. Red indicates shallower depths and blue indicates deeper ocean bottom depths.

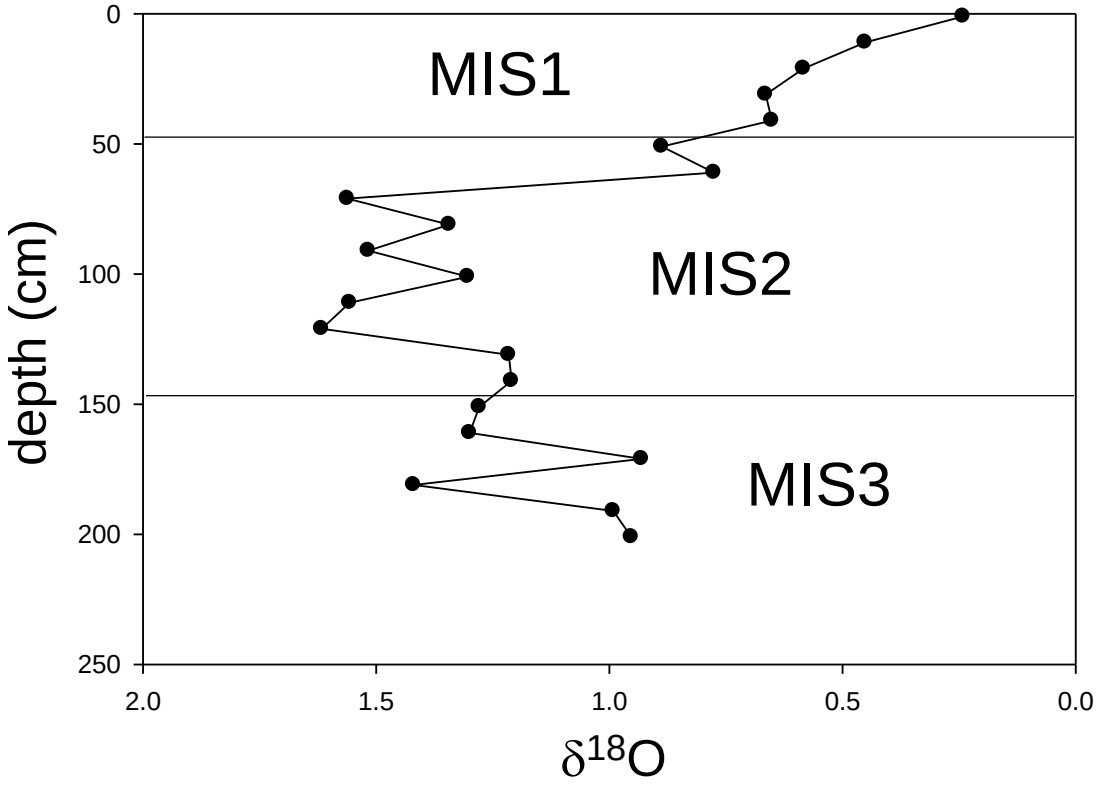

Figure 2. Oxygen isotope record of piston core 11JC.
Marine Isotope Stage (MIS) 1 and 2 boundary at 48 cm indicates end of Last Glacial Maximum (LGM) and beginning of Holocene and MIS2-MIS3 boundary at 147cm depth indicates beginning of LGM. Sedimentation rate during MIS 2 is twice the rate during MIS 1.

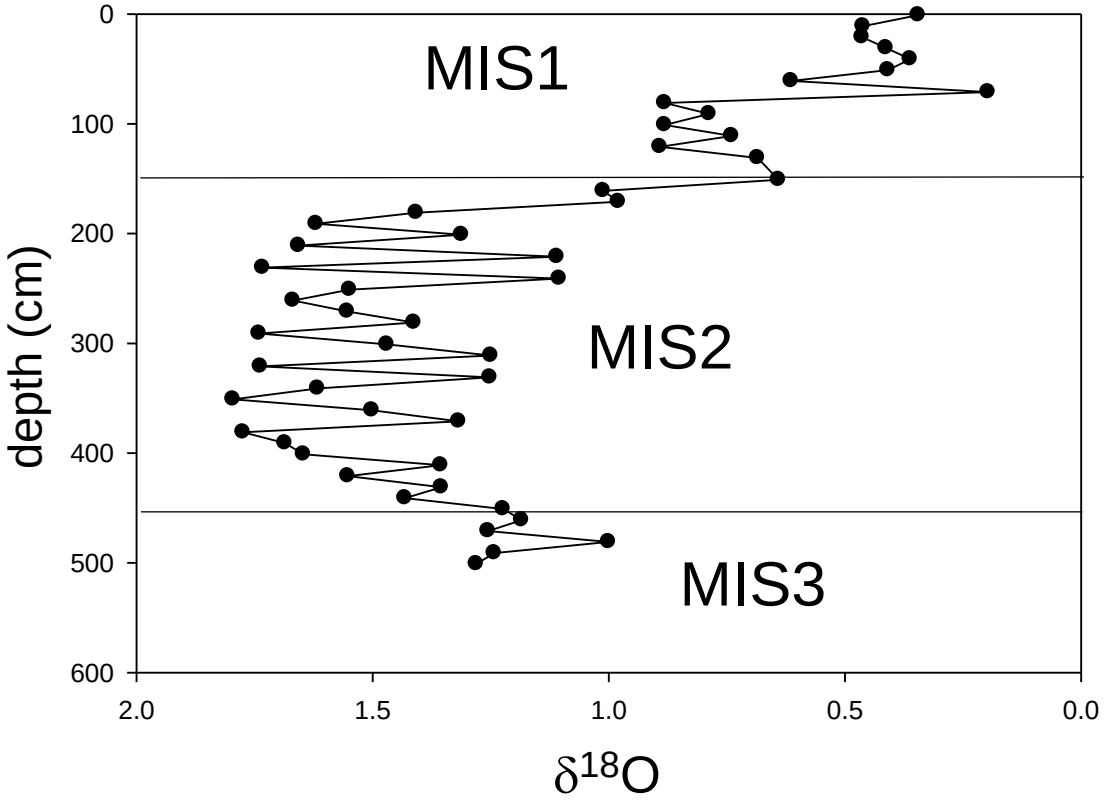

Figure 3. Oxygen isotope record of piston core 17JC.
Marine Isotope Stage (MIS) 1 and 2 boundary at 148 cm indicates end of Last Glacial Maximum (LGM) and beginning of Holocene and MIS2-MIS3 boundary at 436cm depth indicates beginning of LGM. Sedimentation rate during MIS 2 is twice the rate during MIS 1.

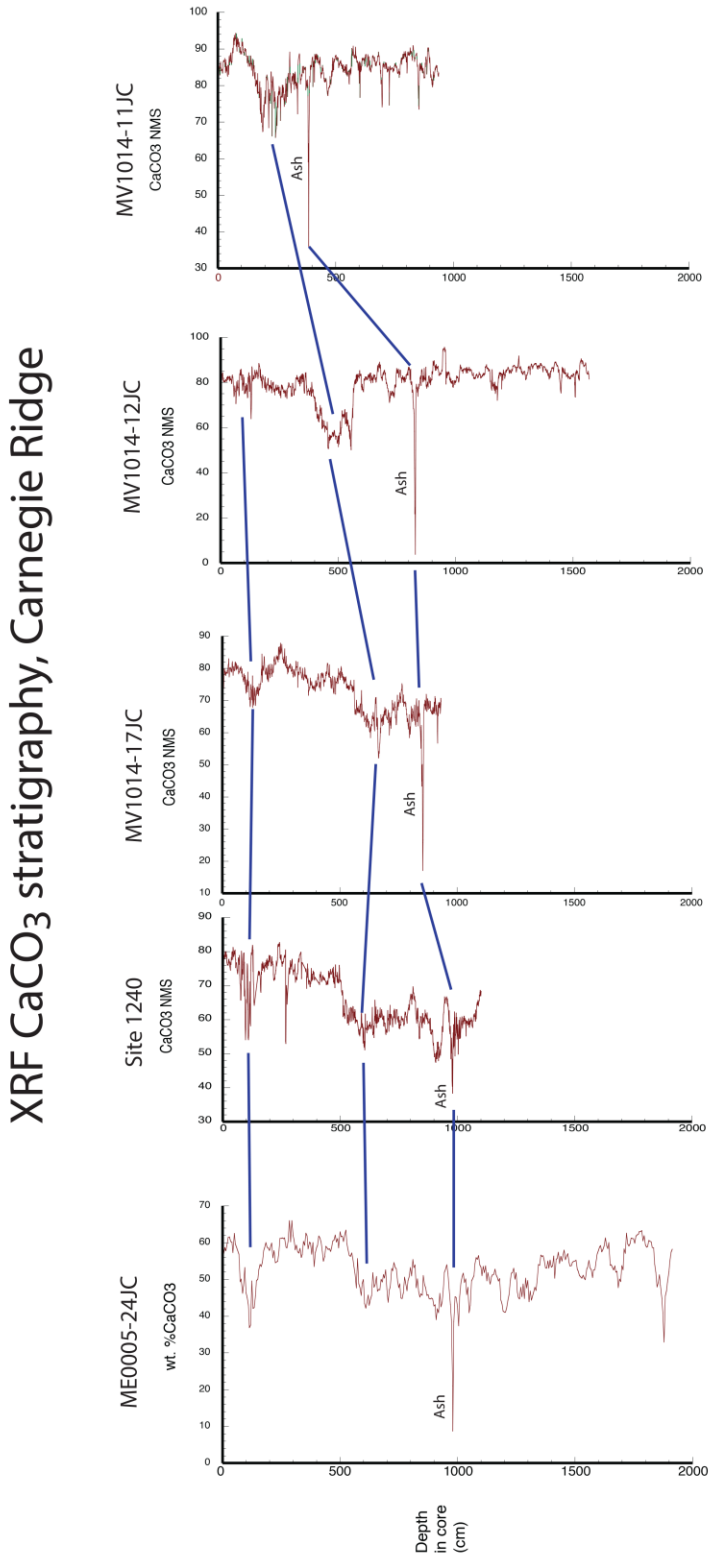

Figure 4. XRF Ca – $CaCO_3$ correlative stratigraphy at Carnegie Sites in the Panama Basin. Ash layer dated to be 84 kya is used as a tie point for chronostratigraphy of these cores

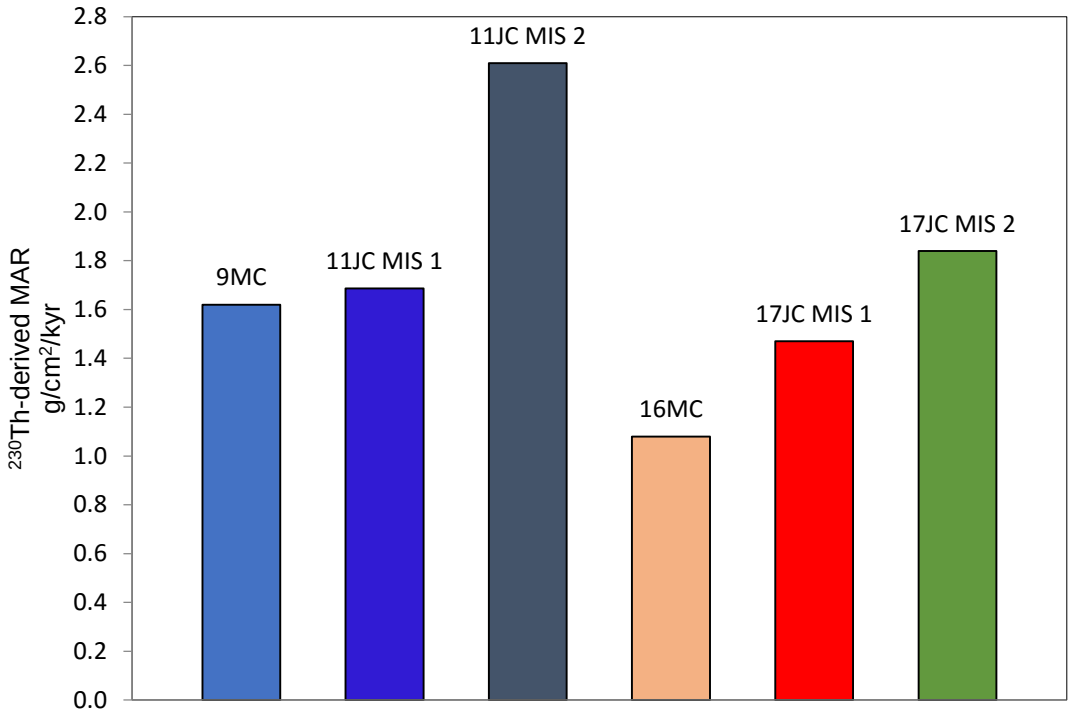

Figure 5. ^{230}Th-derived MARs.
MIS 2 has a temporal increase of MARs for both core sites. Sites 11JC has roughly 30% higher values than downslope 17JC.

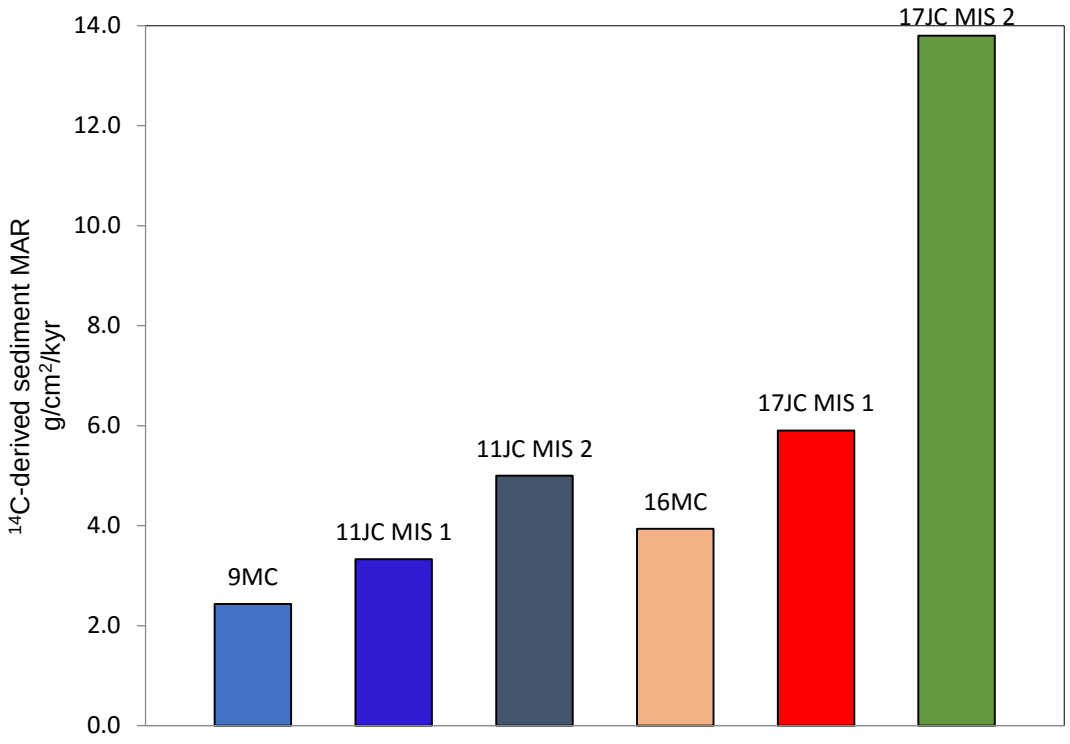

Figure 6. Age-model-derived sediment MARs.
MIS 2 has a temporal increase of MARs for both core sites. Sites 17JC has roughly 250-300% higher values than upslope 11JC.

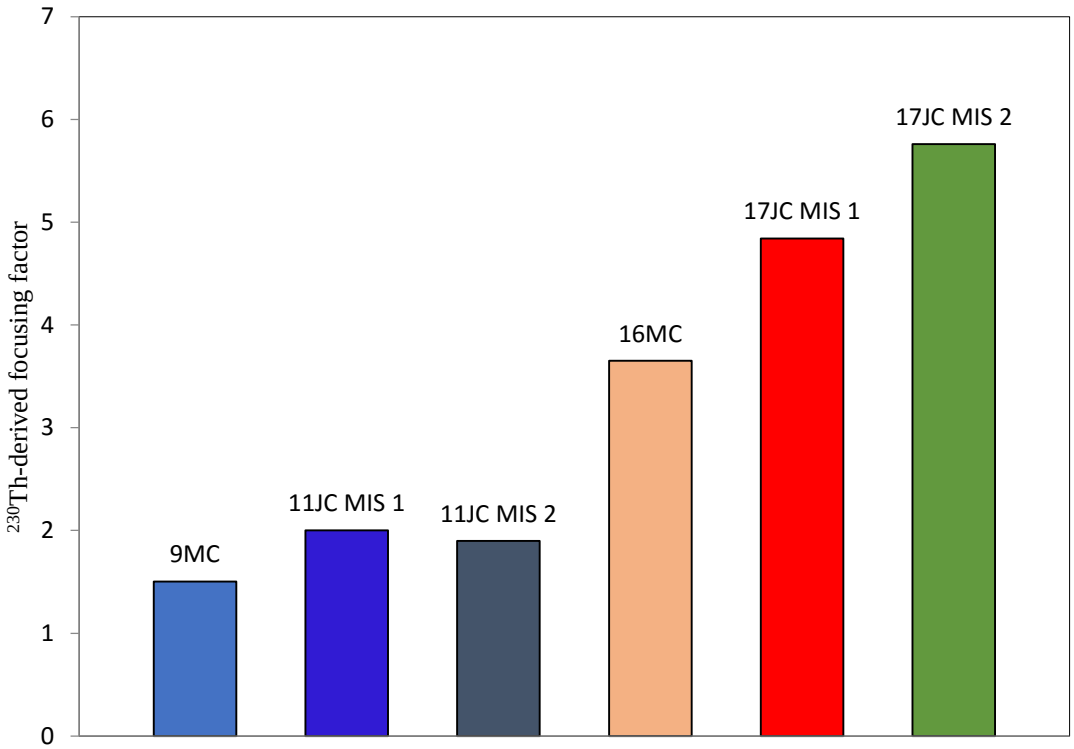

Figure 7. Sediment focusing factors.
Expected focusing at downslope 17JC is seen, and definitively higher values than 11JC, which also shows sediment focusing.

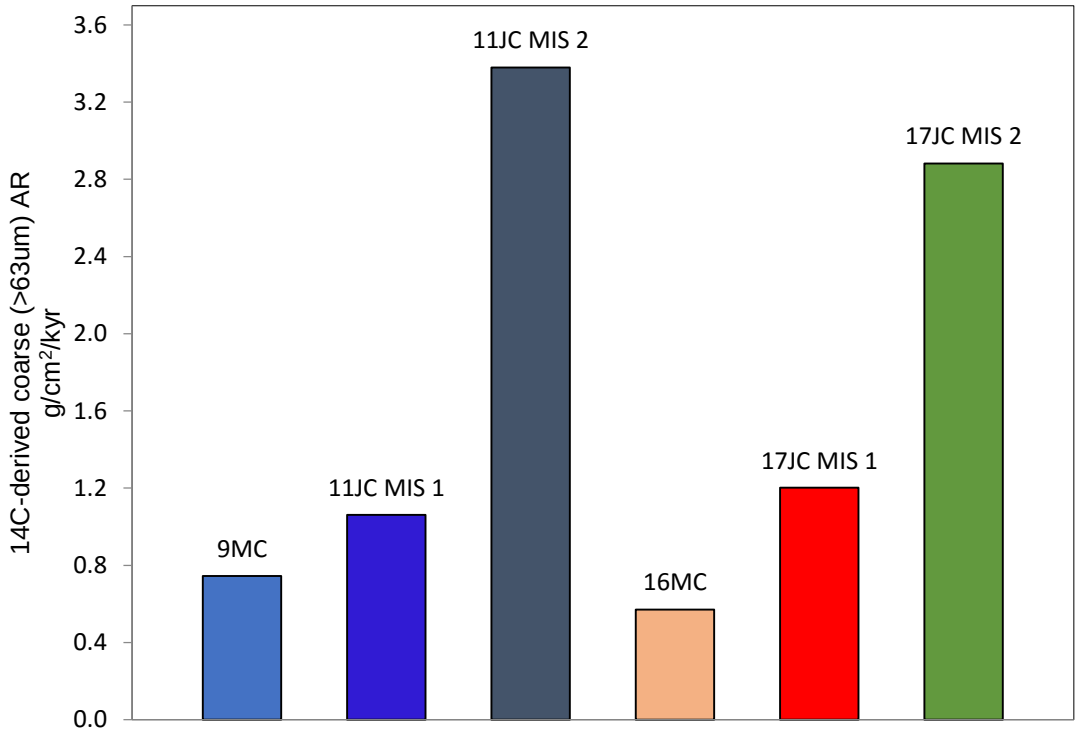

Figure 8. Age-model-derived coarse content accumulation rates.
Temporal and spatial similarities expected to be seen are shown in both cores. Higher productivity during MIS 2 indicated.

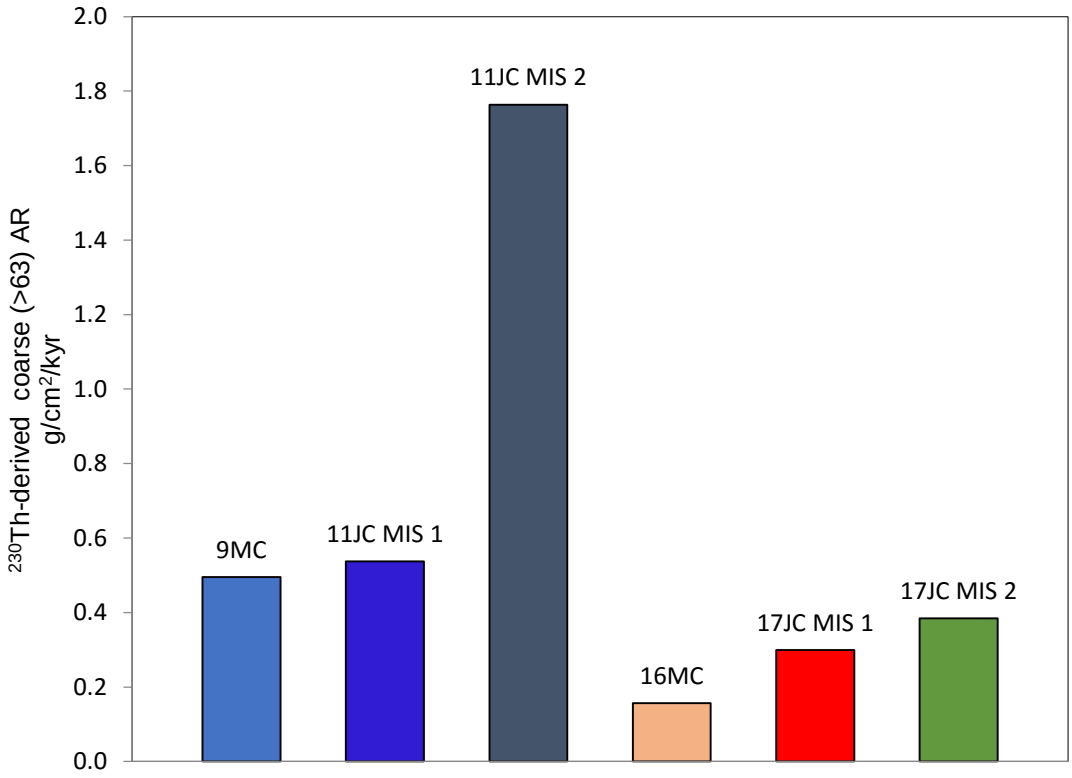

Figure 9. ^{230}Th-normalized coarse content accumulation rates.
Expected MIS 2 increase is seen, however higher core 11JC MIS 2 values indicate 230Th inconsistency with expected result if Constant Flux Proxy (CFP) method was the correct method.

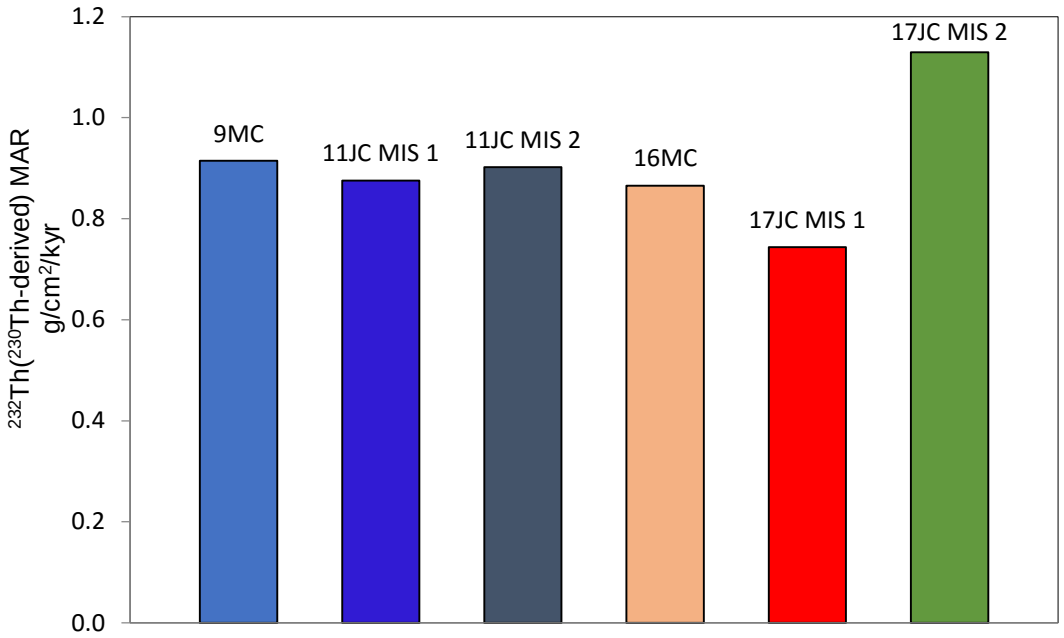

Figure 10. ^{230}Th-derived ^{232}Th accumulation rates.
Dust flux (<10 µm) is accurately measured using 230Th, as variability between cores is no greater than 35%, and 17JC is consistently only has 16-20% variability spatially with core 11JC.

APPENDIX B TABLES

This appendix includes tables to be used in conjunction with the text.

Table 1. Cores from the Melville cruise and other studies.
MV = Melville cruise, MC = multicore, JC = jumbo piston core.

Core ID	Latitude	Longitude	Water Depth (m)
MV1014-02-09MC	00° 41.630’ S	85° 19.996’ W	2452
MV1014-02-11JC	00° 41.630’ S	85° 19.996’ W	2452
MV1014-02-12JC	00° 28.2539’ S	86° 02.9205’ W	2821
MV1014-02-16MC	00° 10.8297’ S	85° 52.0042’ W	2486
MV1014-02-17JC	00° 10.8297’ S	85° 52.0042’ W	2486
ME0005-24JC	00° 01.302’ N	86° 27.788’ W	2941

Table 2. Oxygen isotope tie points for piston cores 11JC and 17JC.

Core ID	Core Top Age (ybp)	MIS1-MIS2 boundary	MIS2-MIS3 boundary
MV1014-02-11JC	5049	48	147
MV1014-02-17JC	2000	148	436

Table 3. Oxygen isotope age model data.
Interpolated using constant sedimentation rates between tie points) for piston cores 11JC and 17JC. End of MIS 2 and beginning of Holocene is 11.5 kya, and beginning of MIS 2 is 25 kya.

CORE	Depth (cm)	Age model (yr)
11JC	1	5049
	11	6527
	21	7871
	31	9215
	41	10559
	51	11903
	61	13166
	71	14428
	81	15691
	91	16954
	101	18216
17JC	1	2000
	21	3348
	41	4632
	61	5916
	81	7199
	101	8483
	121	9767
	141	11051
	161	12127

Table 3. Continued

Depth (cm)	Age model (yr)
181	12995
201	13863
221	14731
241	15599
261	16467
281	17335
301	18203
321	19071
341	19939
361	20807
381	21675
401	22543
421	23411
441	24279
461	25147

Table 4. Comparison of ^{230}Th-derived and age-model-derived bulk and coarse-grained accumulation rates.

Core ID	AR (g cm^{-2} kyr^{-1})				Coarse-grained (>63μm) AR (g cm^{-2} kyr^{-1})			
	^{230}Th-derived		Age-Model-derived		^{230}Th-derived		Age-Model-derived	
	MIS I	MIS II	MIS I	MIS II	MIS I	MIS II	MIS I	MIS II
9MC	1.6	-	2.4	-	0.50	-	0.74	-
16MC	1.1	-	3.4	-	0.16	-	0.50	-
11JC	1.7	2.6	3.3	5.0	0.54	1.8	1.1	3.4
17JC	1.5	1.8	7.1	13.8	0.30	0.38	1.5	2.9

Table 5. Grain size fractionation.
Coarse rate increases two-fold from MIS 1 to MIS 2 does not match focusing in other data.

Core ID	Depth (cm)	Coarse %	MIS 1 and 2 Averages
11JC	0-2	32.7	31.9
	10-12	27.5	
	20-22	35.5	
	60-62	58.1	67.6
	70-72	77.2	
	80-82	67.4	
17JC	0-2	18.5	20.4
	60-62	21.5	
	140-142	21.2	
	260-262	20.9	20.9
	300-302	19.6	
	320-322	22.2	

Table 6. ^{230}Th-derived focusing factors.
Focusing Factors (FF) at 11JC are consistently 2, indicating sediment focusing, in agreeance with 9MC. Downslope 17JC shows expected increase in FF over upslope 11JC. 11JC does not show expected increase in productivity during MIS 2, as shown in core 17JC during MIS 2.

Core ID	FF MIS I	FF MIS II	FF (Glacial/Holocene)
9MC	1.5	-	-
16MC	3.7	-	-
11JC	2.0	1.9	1.0
17JC	4.8	5.8	1.2

Table 7. Data

CORE	Depth (cm)	xs^{230}Th$_{(o)}$[a] (dpm g^{-1})	^{232}Th (µg g^{-1})	^{230}Th-derived MAR[b] (g cm^{-2} kyr^{-1})	U$_{authigenic}$[a] (µg g^{-1})
11JC	1	4.38	0.57	1.50	0.37
	11	4.56	0.61	1.39	0.90
	21	3.96	0.60	1.54	2.83
	31	3.23	0.49	1.83	2.19
	41	2.65	0.38	2.18	2.72
	51	2.14	0.33	2.58	2.24
	61	2.15	0.33	2.49	3.02
	71	1.64	0.32	3.02	3.72
	81	1.49	0.35	3.06	3.53
	91	2.04	0.44	2.20	2.27
	101	1.83	0.44	2.30	2.08
17JC	1	7.08	0.70	1.07	0.54
	21	7.18	0.68	1.06	1.71
	41	6.72	0.68	1.13	3.19
	61	4.90	0.49	1.55	3.33
	81	3.97	0.44	1.92	5.30
	101	4.56	0.40	1.67	4.87
	121	5.13	0.47	1.48	4.35
	141	4.00	0.39	1.90	6.18
	161	3.79	0.37	2.00	7.03

Table 7. Continued

Depth (cm)	$xs^{230}Th_{(o)}$[a] (dpm g^{-1})	^{232}Th (µg g^{-1})	^{230}Th-derived MAR[b] (g cm^{-2} kyr^{-1})	$U_{authigenic}$[a] (µg g^{-1})
181	3.33	0.44	2.28	9.40
201	3.37	0.58	2.26	11.48
221	3.36	0.54	2.26	12.29
241	3.36	0.56	2.26	10.42
261	3.91	0.59	1.94	10.26
281	4.56	0.68	1.67	10.93
301	5.50	0.80	1.38	10.06
321	4.32	0.69	1.76	10.74
341	4.70	0.82	1.62	9.24
361	4.83	0.66	1.57	6.25
381	4.73	0.69	1.61	6.88
401	4.89	0.76	1.55	8.09
421	4.77	0.75	1.59	7.02
441	4.91	0.73	1.55	7.20
461	4.17	0.62	1.82	8.22